

# Summary of Experimental Top Quark Results

**Gordon Watts**

*Department of Physics  
University of Washington  
PO Box 351560  
Seattle, WA 98195-1560 USA  
Email: gwatts@fnal.gov*

ABSTRACT: Recent experimental top quark results are described, including recent updates to the  $t\bar{t}$  cross section. The current world average top mass is  $174.3 \pm 5.1 \text{ GeV}/c^2$ . Also discussed are direct measurements of many properties of the top quark, including the invariant mass of the  $t\bar{t}$  system, the top quark's  $p_T$  distribution, and spin correlations between the  $t$  and  $\bar{t}$ . Measurements of the top quark decay properties have also been made.

## 1. Introduction

Three years have passed since the Top quark has been discovered [2] [3]. Since the discovery both collider detectors at Fermilab's Tevatron have made top quark physics a new field of study. The top quark is much more massive than any of the other quarks in the Standard Model (SM). Indeed, if the Super-Kamiokande results are taken into account [23], over twelve orders of magnitude in mass exist in the SM:  $0 < m_\nu < 10^{-12}m_t$ . The large top quark mass also allows experimenters several unique handles in SM physics. Because  $m_t \gg m_W$ , real  $W$  bosons are produced in the top quark decays. Also, the top quark width is greater than  $\Lambda_{\text{QCD}}$ , so the top quark does not hadronize to form toponia but, rather, decays as a bare quark. Finally, a number of models, such as gravity based SUSY models, have shown that top quark production and decay properties are an excellent place to search for evidence of physics beyond the SM.

With the data taken at the Tevatron in Run 1 ( $\approx 120 \text{ pb}^{-1}$ ) both experiments have begun to probe the SM. The top quark's production cross section and mass have been well measured by both experiments, as summarized below. Both experiments have begun an ambitious program measuring the decay properties of the top quark, including the  $t\bar{t}$  invariant mass, the top quark's

$p_T$  distribution, and spin correlations between the two top quarks (many other topics have been investigated, but not reported here) [1]. These investigations will continue in the next data taking run at the Tevatron, Run 2, currently scheduled to start in 2001.

### 1.1 Production and Decay of the Top Quark at the Tevatron

In the SM a top quark decays almost exclusively via  $t \rightarrow Wb$ . The decay is classified by the decay products of the two  $W$ 's, as outlined in table 1.

Both the dilepton and lepton + jets channels include  $\tau$  decays, which are difficult to individually identify in the DØ and CDF detectors. Both experiments have looked in the dilepton channels for decays involving a  $\tau$  but the lepton+jets channels remain uninvestigated.

In all channels other than the dilepton channel it is necessary to identify the  $b$  quark in the decay in order to reduce the backgrounds to manageable levels. There are two ways to tag a jet containing a  $b$  quark. First, its decay frequently contains a soft lepton (from either the  $B$  meson decay, or a cascade decay thru a  $D$  meson or  $K$  meson). Second, the highly boosted  $B$  meson has an average  $c\tau$  of  $453 \mu\text{m}$ . It decays with an average of 5.75 charged particle tracks [22]. The Silicon Vertex Detector at CDF can tag the resulting displaced vertex.

| Decay Channel | Products                    | BF  | Backgrounds                              |
|---------------|-----------------------------|-----|--|
| All Jets      | $jjjjbb$                    | 44% | QCD                                      |
| Lepton + Jets | $\uparrow\nu jjbb$          | 30% | $Wbb$ , $W$ +jets, $Z$ +jets, QCD, fakes |
| Dilepton      | $\uparrow\nu\uparrow\nu bb$ | 5%  | fakes, Drell-Yan                         |

**Table 1:** The top quark decay channels, decay products, branching fractions, and principle backgrounds. The  $\tau$  decay channels are not included here, as they are difficult to identify with the present detectors.

Details of the analysis and the selection cuts are described in the papers [5] and [6].

## 2. The Cross Section

Both CDF and DØ measure the  $t\bar{t}$  cross section in the lepton+jets channel, the all hadronic channel, and the dilepton channel. The cross section measurement was how the discovery of the top quark was made.

Table 2 shows the current event samples for CDF and DØ. The lepton+jets channel is divided into three classes. CDF takes advantage of their SVX detector to tag jets containing  $b$ 's, while DØ relies more heavily on kinematic variables.

### 2.1 Update of the Combined Cross Section Measurement

CDF recently completed a detailed study of its  $b$ -tagging fake rates for their SVX tagging algorithm [4]. To summarize, CDF starts by looking at tracks in a jet. It uses tracks that do not intersect the primary vertex (displaced tracks) as a starting point to try to fit a secondary vertex. The distance between the primary and secondary vertex is called the decay length. See figure 1a. To calculate the fake rate due to detector mismeasurement for this algorithm, CDF uses so-called negative decay length vertices: those that occur behind the primary vertex with respect to the direction of the jet. The other source of fake tags for top events is, of course, irreducible physics processes like  $W \rightarrow b\bar{b}$  and  $g \rightarrow b\bar{b}$ . Their contributions must be carefully calculated.

CDF has found that when two  $b$  quark jets decay within a single reconstructed jet to each other they can produce a negative decay length secondary vertex, as shown in figure 1b. This can happen when a  $g \rightarrow b\bar{b}$  decay occurs and the two  $b$ 's are sufficiently collinear. In the previous

method of calculating the  $b$ -tagging background this lead to some double counting, as one source of fake tags was also accounted for in the real physics backgrounds. The mistag rate dropped by 20-50% (it is a function of jet  $E_T$ ), and the associated error dropped from 40% to 10%.

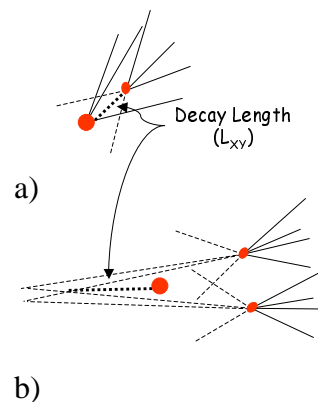


**Figure 1:** The SVX  $b$ -tag algorithm. (a) shows a standard single  $b$  decay and how it is reconstructed. (b) shows how a negative decay length vertex can be found when two  $b$ 's from gluon splitting decay within a single reconstructed jet. The large solid circle represents the primary interaction vertex, the smaller circle the secondary vertex where the  $b$  has decayed.

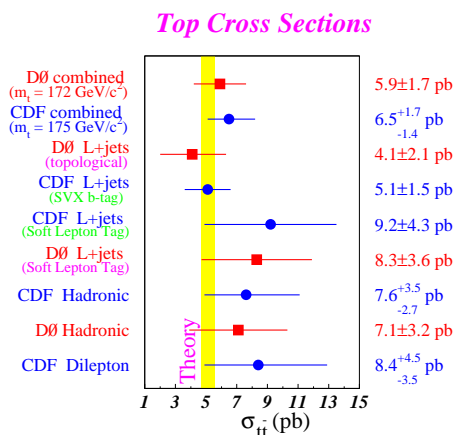
### 2.2 Tevatron $t\bar{t}$ Cross Section Results

Figure 2 shows the most recent results of the cross section measurement from both experiments.

The Tevatron Run 2 will upgrade many components of the detector and accelerator at FNAL. In particular, the Tevatron energy will increase from  $\sqrt{s} = 1.8$  TeV to  $\sqrt{s} = 2.0$  TeV, resulting in a 40% increase in the  $t\bar{t}$  cross section. Silicon vertex detectors will be added to both experiments; they will cover a much larger fiducial region than CDF's Run 1 SVX. This along with better geometry (more layers, stereo layers, etc.) will increase the  $b$ -tagging efficiency

| Channel                       | DØ     |                | CDF    |                |
|-------------------------------|--------|----------------|--------|----------------|
|                               | Events | Background     | Events | Background     |
| All-Jets                      | 41     | $24.8 \pm 2.4$ | 187    | $142 \pm 12$   |
| Lepton+Jets (SVX $b$ -tag)    |        |                | 34     | $9.2 \pm 1.5$  |
| Lepton+Jets (Lepton $b$ -tag) | 11     | $2.4 \pm 0.5$  | 40     | $22.6 \pm 2.8$ |
| Lepton+Jets (Topological)     | 19     | $8.7 \pm 1.7$  |        |                |
| Dilepton                      | 5      | $1.4 \pm 0.4$  | 9      | $2.4 \pm 0.5$  |
| $e\tau, \mu\tau$              |        |                | 4      | $\approx 2$    |
| $e\nu$                        | 4      | $1.2 \pm 0.4$  |        |                |

**Table 2:** The number of observed events and backgrounds in each top quark decay channel. The Lepton+jets topological channel uses cuts on event energy ( $H_T$ ) and Aplanarity. The  $e\nu$  analysis is sensitive to  $\tau$ , dilepton, and lepton+jets events that fail the standard analysis.



**Figure 2:** Tabulation of the cross section results for all the channels from both DØ and CDF. The theory band is derived from the mass measurement and the NLO cross section calculation by [9].

dramatically. Other improvements include lepton id and tracking. Finally, in Run 2a alone, almost  $2 \text{ fb}^{-1}$  are expected. Table 3 shows the expected event yields. The larger event samples will make possible better cross section measurements ( $\approx 11\%$  per experiment).

| Channel                       | Yield |
|-------------------------------|-------|
| Dilepton                      | 150   |
| Lepton + Jets SVX Tag         | 1000  |
| Lepton + Jets Double SVX Tags | 300   |

**Table 3:** Expected yields for each experiment in Run 2a. The Tevatron expects to deliver  $2 \text{ fb}^{-1}$  to each experiment at  $\sqrt{s} = 2.0 \text{ TeV}$ . In Run 1, CDF observed 9 double tagged lepton+jets events.

### 2.3 Neural Network Analysis of $t\bar{t} \rightarrow e\mu$

DØ has analyzed the data in the  $e\mu$  channel using a neural network based analysis. The dilepton channels have the least background, and the  $t\bar{t} \rightarrow e\mu b\bar{b}\nu\nu$  decay is the golden channel due to the small background rates containing unlike flavors of dileptons. Unfortunately, its branching fraction is also quite small, 2.5%, and so every effort must be made to maximize the selection cuts.

DØ's previously published result [5] required one electron with  $E_T > 15 \text{ GeV}$ , one muon with  $p_T > 15 \text{ GeV}/c$ ,  $\cancel{E}_T > 20 \text{ GeV}$ , two jets with  $E_T > 20 \text{ GeV}$ ,  $\Delta R(e, \text{jet}) > 0.5$  (in  $\eta - \phi$  space),  $\Delta R(e, \mu) > 0.25$  and  $H_T \equiv E_T^e + \sum E_T^{\text{jet}} > 120 \text{ GeV}$ . When the data is analyzed [11], the  $H_T$  requirement is removed and the jet  $E_T$  and  $\cancel{E}_T$  requirements are reduced to 15 GeV.

The required background rejection is achieved with a neural network selection cut. The major backgrounds in this channel are QCD jet production,  $Z \rightarrow \tau\tau \rightarrow e\mu$ , and  $WW \rightarrow e\mu$ . One network is trained to distinguish signal from a particular background. Each of the networks uses six variables for input:  $E_T^e$ ,  $E_T^{\text{jet}2}$ ,  $\cancel{E}_T$ ,  $H_T^{\text{jets}}$ ,  $M_{e\mu}$ , and  $\Delta\phi_{e\mu}$  (the  $Z \rightarrow \tau\tau$  network uses  $E_T^{\text{jet}1}$  instead of  $E_T^{\text{jet}2}$ ). Each of the three networks are trained on an equal number of background and signal events, 4000 for the QCD network, and 2000 events for the other two.

The outputs  $O_i$  are combined using the relation  $3O_{\text{comb}}^{-1} = \sum_{i=1}^3 O_i^{-1}$ . The cut on  $O_{\text{comb}}$  is determined to be 0.88 by maximizing the expected relative significance  $S/\sigma_B$ , as shown in figure 3.

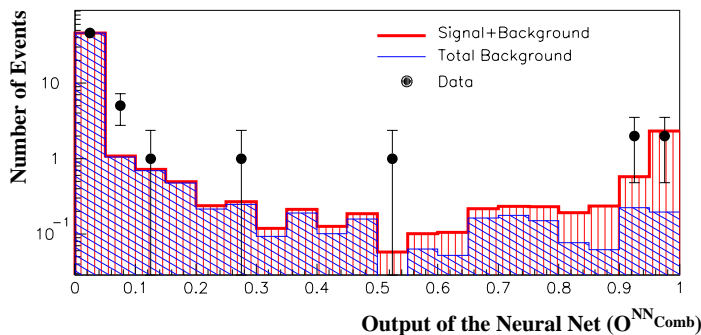


**Figure 3:** The output of the neural net,  $O_{\text{comb}}$  in the search for  $t \rightarrow e\mu$ . The bold hatched histogram represents the output of the NN when run on signal and background, and the second histogram represents the output for all backgrounds. The NN output is peaked near one for the signal.

The results are shown in table 4. Compared to the published analysis, the neural network analysis has improved efficiency by about 10%. The background is slightly lower, but it is difficult to evaluate due to the large statistical uncertainty. It is important to note that the neural network technique will likely play a large roll in analysis and searches during the Tevatron’s Run 2. In the early part of the run these techniques may be used to extract as clean a sample of  $t\bar{t}$  decays as possible in order to accurately measure the mass.

|                                  | NN Analysis              | Conventional             |
|----------------------------------|--------------------------|--------------------------|
| $\epsilon \times \text{BR} (\%)$ | $0.402 \pm 0.085$        | $0.368 \pm 0.078$        |
| Background Observed              | $0.24 \pm 0.15$          | $0.26 \pm 0.16$          |
| Events                           | 4                        | 3                        |
| $\sigma(t\bar{t})$               | $8.8 \pm 5.1 \text{ pb}$ | $7.1 \pm 4.8 \text{ pb}$ |

**Table 4:** Results from the  $e\mu$  dilepton neural net analysis (NN) compared with the conventional analysis. The neural net analysis has better acceptance, however, statistics are limited enough that it is hard to evaluate.

### 3. The Top Quark Mass

Arguably the best measurement made of the top quark to date is its mass. The top quark mass is a fundamental parameter of the SM; once it is determined the remaining properties of its decay can be predicted. This provides a valuable test of the SM. It also participates in the radiative corrections for the Higgs. The measurement of

its mass along with the  $W$  boson mass and other electroweak parameters allows one to calculate a constraint of the SM Higgs mass.

Measurements have been made in all channels: dilepton, all-jets, and lepton+jets. Both experiments have published detailed papers on the mass measurements in [7] and [8]. The results are summarized and tabulated in figure 4. Both CDF and DØ have combined their top mass measurements, properly accounting for the correlated errors [10]. The Tevatron Top Mass is  $m_t = 174.3 \pm 5.1 \text{ GeV}/c^2$ .

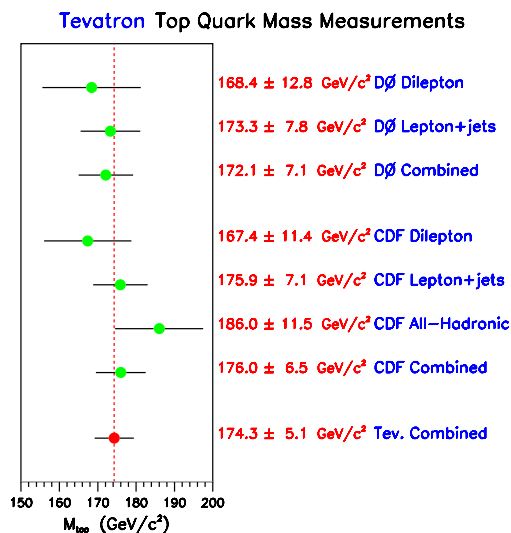


**Figure 4:** A plot representing the top quark mass measurements in all the published channels from both CDF and DØ. The bottom most point is the combined mass.

Figure 5 shows the present direct measure-

ments of  $m_t$  from the Tevatron, and  $m_w$  from the Tevatron and LEP2, along with indirect measurements from LEP1, SLD, and deep inelastic neutrino scattering ( $\nu N$ ). A SM fit of the electroweak parameters and the top quark mass gives a Higgs mass of  $m_H = 97_{-38}^{+57}$  [24].

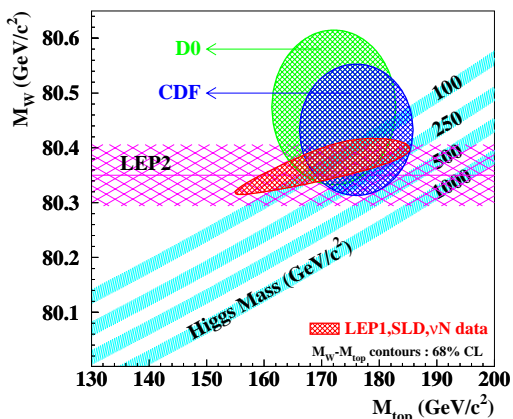


**Figure 5:** The results of an electroweak fit to the SM parameters as a function of the top mass ( $m_t$ ) and the  $W$  mass ( $m_W$ ). CDF and DØ direct measurement of both (including errors) are shown separately, along with LEP2’s direct measurement of the  $W$  mass. Indirect measurements from LEP1, SLD, and  $\nu N$  area also shown. The data favors a light Higgs mass.

Table 5 shows the contributions to the systematic errors in the two experiments. The largest systematic error is the Jet Energy Scale (JES). The dilepton mass measurement depends less on the JES than the lepton+jets, though its BR is smaller. In Run 1 the dilepton mass measurement had the largest statistical error and the smallest systematic error. In Run 2 the situation will change, as the mass measurement is likely to be dominated by the systematic errors instead of statistical. New detectors and improved jet measurements should help reduce that error as well. The top mass error predicted for Run 2 is  $\approx 3\text{GeV}/c^2$  for each experiment, which along with the better cross section measurement will help to further constrain the SM. Also, along with the expected  $\delta m_W$  of  $40\text{MeV}/c^2$ , each experiment should be able to predict  $\delta m_{\text{Higgs}} = 40\%$ .

### 3.1 Mass of the $t\bar{t}$ System

Both CDF and DØ have looked at the mass of

|                   | l+jet      |            | dilepton    |             |
|-------------------|------------|------------|-------------|-------------|
|                   | CDF        | DØ         | CDF         | DØ          |
| <b>Stat Error</b> | <b>4.8</b> | <b>5.6</b> | <b>10.3</b> | <b>12.3</b> |
| JES               | 4.4        | 4          | 3.8         | 2.4         |
| Signal Model      | 2.6        | 1.9        | 2.8         | 1.7         |
| <b>Total Sys</b>  | <b>5.3</b> | <b>5.5</b> | <b>4.8</b>  | <b>3.6</b>  |
| $m_t$             | 175.9      | 173.3      | 167.4       | 168.4       |
| % Stat Error      | 2.7        | 3.2        | 6.1         | 7.3         |
| % Sys Error       | 3          | 3.1        | 2.8         | 2.1         |

**Table 5:** Systematic and statistical errors on the  $m_t$  measurement for both DØ and CDF. The errors and masses are all listed in  $\text{GeV}/c^2$ .

the  $M_{t\bar{t}}$  system. A peak is expected if the  $t\bar{t}$  system is decaying from another object, such as a  $Z'$ . Results are shown in figure 6. The selection of events is the same as their mass analysis, except their fit  $\chi^2$  is loosened and the top mass is constrained to be  $127\text{GeV}/c^2$ . They also remove the constraint and calculate the 3 body mass of each system and it must be between 150 and 200  $\text{GeV}/c^2$  to suppresses wrong combinations. DØ has performed a similar analysis and its results can also be seen in figure 6.

## 4. Single Top Searches

Single top production at the Tevatron provides an opportunity to study the charged-current weak-interaction of the top-quark; a way to directly measure  $V_{tb}$ . It is also sensitive to the non-standard  $Wtb$  vertex and to exotic single-top-production processes [25]. Figure 7 shows two production processes searched for by CDF. Details of their searches can be found in the paper [26]. Generically, the single-top cross section is about a factor of 5 lower than top quark pair production cross section, and, is topologically similar to many of the same backgrounds (including  $t\bar{t}$ ).

The quark jet in  $W$ -gluon fusion is expected to be energetic and the  $b$  quark is expected to be soft. Since  $t\bar{t}$  production makes large contributions to the  $W+3$  jets signal, only the  $W+2$  jets samples are searched (the third jet is removed with an  $E_T < 15\text{GeV}$  cut). This reduces the acceptance by a half, but the  $t\bar{t}$  contribution by 85%. A mass window cut,  $145 < M(\uparrow\nu b) < 205$

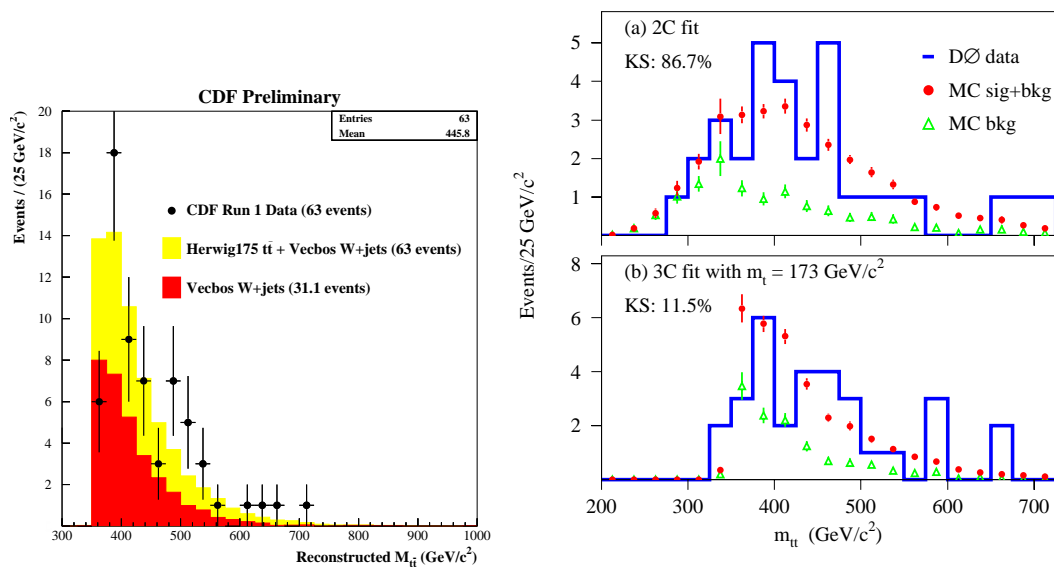


**Figure 6:** The invariant mass distribution for  $t\bar{t}$  ( $M_{t\bar{t}}$ ). CDF’s results are shown on the right. The points are the data, the light histogram is Monte Carlo + background and the darker histogram is background only. DØ’s  $M_{t\bar{t}}$  is shown on the left. The lower plot requires that the top mass be the measured 173 GeV/c<sup>2</sup>. The histogram is the data, the upper points are MC + background, and the lower points are background only.

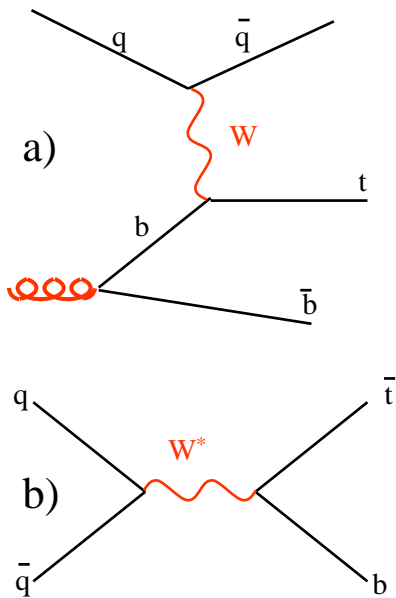


**Figure 7:** Feynman diagrams for the production of single-top. The first, a), is t-channel production (so called  $W$ -gluon fusion) and the second, b), is s-channel (so called  $W^*$  production) production.

GeV/c<sup>2</sup>, is further required. A single SVX  $b$  tag is also required. Results are summarized in table 6.

The  $W^*$  channel is more difficult because the second  $b$  quark jet is expected to be energetic. The key discriminating variable is  $M(\downarrow\nu b)$ . MC studies show that the  $b$  quark with larger pseudo-rapidity is associated with the  $t$  quark decay about 64% of the time. A maximum likelihood method is used to estimate the individual contributions of the background and signal to the observed data sample. The results are summarized in table 6.

## 5. Top Properties

In this section top properties are listed, including spin correlations, the  $p_T$  distribution, and a charged Higgs disappearance analysis.

### 5.1 Spin Correlations

Unique among the quarks, the top quark decays so quickly that the final state interactions do not disturb its spin: the angular distribution of the top quark decay products contain information about its initial spin. Since the top quark is a pair-produced spin-1/2 particle, for a given spin quantization axis a pair of top quarks will have either opposite or identical spins. It is possible

| Channel  | Background     | Signal        | Observed | $\sigma$           |
|----------|----------------|---------------|----------|--------------------|
| W fusion | $12.9 \pm 5.0$ | $1.2 \pm 0.3$ | 15       | $< 15.4$ pb 95% CL |
| $W^*$    | $31.3 \pm 3.9$ | $1.0 \pm 0.3$ | 42       | $< 15.8$ pb 95% CL |

**Table 6:** Expected event production yields, backgrounds, observed events, and cross section limits found in the single-top analysis by CDF.

to calculate the outcome in the framework of the SM, and, indeed, an asymmetry is predicted [19] [20]. Deviation from this calculated value would imply new physics. DØ has carried out an initial measurement in the Run 1 data [18]. The sensitivity is greatest for charged leptons and  $d$ -type quarks [19]. Only dilepton events are considered in this analysis because it is much simpler to identify leptons than  $d$ -type quarks. In this case, both top quarks decay via  $t \rightarrow l\nu b$ .

DØ chooses the *optimal off-diagonal basis* as the spin quantization axis [19]. The angle between the beam axis and the off-diagonal basis,  $\Psi$ , is chosen to give the largest expected spin correlation. The angle between the lepton and the off-diagonal basis,  $\theta_{\pm}$  is defined in the top-quark rest frame. The joint distribution of these two angles is

$$\frac{1}{\sigma} \frac{d^2\sigma}{d(\cos\theta_+)d(\cos\theta_-)} = \frac{1 + \kappa \cos\theta_+ \cos\theta_-}{4}.$$

The spin correlation information is contained in  $\kappa$ ; the SM prediction at  $\sqrt{s} = 1.8$  TeV is  $k \approx 0.9$ .

It is not possible to solve directly for  $\theta_{\pm}$ , unfortunately, because a  $t\bar{t}$  dilepton event is kinematically under constrained (due to the two neutrinos in the final state). DØ uses the same set of techniques it developed for the mass measurement to derive probability distributions for  $\theta_{\pm}$  [21]. There are six dilepton candidates with an expected background of  $1.5 \pm 0.3$  events in their Run 1 data sample. The distribution of solutions in  $(\theta_+, \theta_-)$  is calculated and plotted in a 2D histogram for each event. Figure 8 shows the result after each event's 2D histogram is summed together. Statistics from Run 1 are not sufficient to provide a significant measurement of  $\kappa$ , DØ finds that  $\kappa > -0.25$  at 95% confidence.

In Run 2, DØ expects to collect 150 dilepton events, and should be able to discriminate between  $\kappa = 0$  and  $\kappa = +1$  at the  $2.5\sigma$  level.

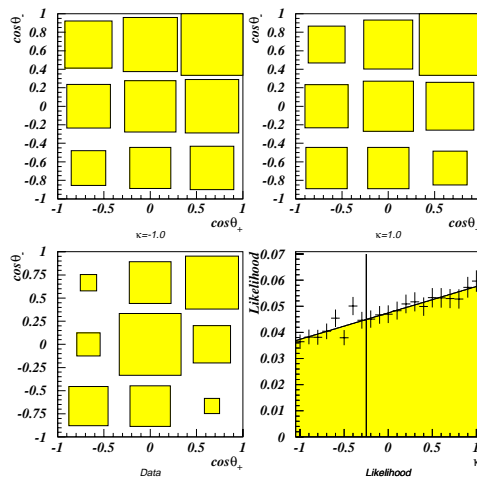


**Figure 8:** Results of the  $t\bar{t}$  spin correlation analysis. The upper two plots show the  $\cos\theta_+$  vs.  $\cos\theta_-$  scatter for MC data when the decay products are fixed to have  $\kappa = \pm 1$ . The lower left hand plot shows DØ's data. The final lower right hand plot is the result of fitting the data to MC expectations to derive a likelihood as a function of  $\kappa$ .

## 6. Top $p_T$ Distributions

A wide variety of new physics can lead to enhancement of the differential top cross section at high  $p_T$ . A new strong interaction, top color for example, will alter the top  $p_T$  distribution [16], or the low scale quantum gravity model proposed by Arkani-Hammed *et al.* [27]. In fact, the shape of the  $p_T$  distribution is one of the most sensitive variables to new physics [17].

CDF has extracted and compared the top  $p_T$  distribution in their data and compared it to the SM expectation [28]. Top events are extracted from the lepton+jets channel. Events with a central ( $|\eta| < 1.0$ ) electron with  $E_T > 20$  GeV or a muon with  $p_T > 20$  GeV,  $\cancel{E}_T > 20$  GeV, at least three jets with  $|\eta| < 2.0$  and  $E_T > 15$  GeV, and a fourth jet with  $E_T > 8$  GeV and  $|\eta| < 2.4$  are selected. To increase the signal to background significance either  $N_{\text{jet } E_T > 15 \text{ GeV}} \geq 4$  or  $N_{\text{tag}} \geq 1$ ,

where  $N_{tag}$  is the number of tagged jets in the event (a jets is tagged if there is a soft-lepton or secondary vertex associated with the jet). A kinematic fit is applied to the sample, with the top mass fixed to the measured value, and a cut applied to the  $\chi^2$ . 61 events remain, 29 of them have  $b$ -tags. Background in the sample is estimated to be  $24.6 \pm 5.8$  by doing a likely hood fit to the number of events in zero tag, single tag, and double-tagged subsamples.

The top quark  $p_T$  is split into 4 bins: 0-75, 75-150, 150-225, and 225-300 GeV/c. The acceptance for each bin is calculated separately (the high  $p_T$  quark acceptance is higher). The differential cross section is determined using an unbinned likelihood fit using MC templates (tagged and untagged events use different templates). The results are shown in figure 9a, and listed in table 7.

| $p_T$ Bin               | $t$ -quark fraction                      |
|-------------------------|--|
| $0 < p_T < 75$ GeV/c    | $R_1 = 0.29^{+0.18+0.08}_{-0.18-0.08}$   |
| $75 < p_T < 150$ GeV/c  | $R_2 = 0.42^{+0.18+0.05}_{-0.18-0.07}$   |
| $150 < p_T < 225$ GeV/c | $R_3 = 0.29^{+0.12+0.06}_{-0.10-0.05}$   |
| $225 < p_T < 300$ GeV/c | $R_4 = 0.00^{+0.035+0.019}_{-0.00-0.00}$ |

**Table 7:** Measured fraction of top quarks as a function of their  $p_T$  bin. The first error is statistical, the second systematic.  $R_4$  is considered most sensitive to new physics.

The highest  $p_T$  bin,  $R_4$  is most sensitive to new physics. Its fit value is zero. To determine the upper bound on  $R_4$  given the statistics, the experiment is repeated many times with different values of  $R_4$  in Monte Carlo, which each results smeared by the systematic error. The value of  $R_4$  is taken where only 5% of the experiments have  $R_4$  equal to zero. Figure 9b shows the resulting limit,  $R_4 < 0.114$  at 95% CL. This is a model independent result and can be compared to any proposed extension to the standard model.

## 7. Higgs Disappearance Analysis

The SM contains a single complex Higgs doublet, and therefore a single physical Higgs boson ( $H^0$ ). Many extensions to the SM add multiple Higgs doublets. Supersymmetry [13], for example, adds two Higgs doublets, giving rise to five physical

Higgs states:  $H^0$ ,  $h^0$ ,  $A^0$ ,  $H^+$ , and  $H^-$ . The electroweak sector is specified, in this model, by  $m_{H^+}$ ,  $m_W$ , and  $\tan\beta$ , where  $\tan\beta$  is the ratio of the vacuum expectation values from the two Higgs doublets. If  $m_{H^+} < (m_t - m_b)$  then the decay  $t \rightarrow H^+b$  can compete with the SM decay  $t \rightarrow Wb$ .

In the regions where  $m_{H^+}$  is small and  $\tan\beta$  is either large or small are regions where  $\text{BR}(t \rightarrow H^+)$  is large, and therefore regions where a collider experiment would be sensitive. Figure 10 shows the regions where DØ is sensitive to the  $t \rightarrow H^+b$  decay. Once the  $H^+$  is produced it can decay to  $\tau\nu$  for large  $\tan\beta$ ,  $cs$  for small  $\tan\beta$ , and for both small  $\tan\beta$  and large  $m_{H^+}$ , however,  $H^+ \rightarrow t^*b \rightarrow Wbb$  is relatively large.

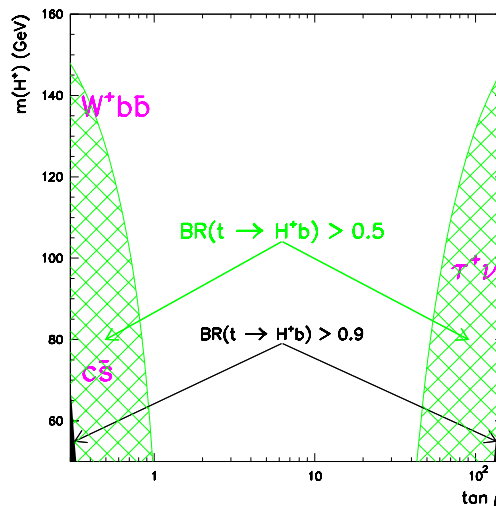


**Figure 10:** Map of the  $m_{H^+}$  and  $\tan\beta$  parameter space. Regions with  $\text{BR}(t \rightarrow H^+b) > 0.5$  are hatched (the charged higgs decay modes in those regions are shown). The dark shaded regions, with  $\text{BR}(t \rightarrow H^+b) > 0.9$ , are not considered.

DØ has searched for the  $t \rightarrow H^+$  decay using a so-called *disappearance analysis* [14]. The results is based on the results of DØ's cross section measurement in the lepton + jets channel [15]. DØ finds 30  $t\bar{t}$  candidates in this channel, with an expected background of  $11 \pm 2$  events.

Regions of parameter space in which  $t \rightarrow H^+$  and then to final states for which DØ has low acceptance can be excluded as the observed excess of signal over background cannot be explained by  $t\bar{t}$  production.

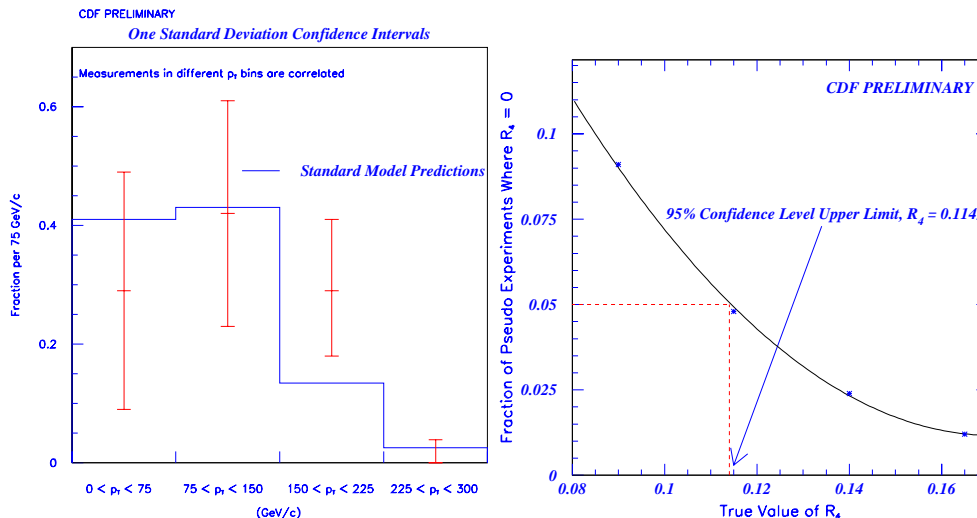


**Figure 9:** The results of the top quark  $p_T$  fit. The left plot is the observed data (points) and SM predictions (histogram) as a function of the 4  $p_T$  bins.  $R_4$  is considered most sensitive to new physics. The righthand plot is the 95% C.L. upper limit on the true value of  $R_4$ .

Assuming the cross section has no contributions from any new physics channels,  $D\bar{O}$  can exclude shaded regions of parameter space shown in figure 11. The analysis is valid only in the central area of the plot; the analysis is invalid on the outside regions of the plot because the perturbative calculations for the Higgs branching ratios are invalid there. LEP already excludes  $M_{H^+} < 60$   $\text{GeV}/c^2$ . In Run 2  $D\bar{O}$  will increase the area excluded by a factor of two.

## References

- [1] Properties of the top quark PRDs
- [2] F. Abe et al., Phys. Rev. Lett. 74, 2626 (1995).
- [3] S. Abachi et al., Phys. Rev. Lett. 74, 2632 (1995).
- [4] F. Ptohos (for the CDF collaboration), proceedings of the International Europhysics Conference on High Energy Physics 99, Tampere, Finland, July 17, 1999.
- [5] Phys.Rev.Lett. 79 (1997) 1203-1208, hep-ex/9704015 and Phys. Rev. Lett. 83 (1999) 1908-1913, hep-ex/9901023.
- [6] Phys.Rev.Lett. 80 (1998) 2779-2784, hep-ex/9802017
- [7] Phys.Rev.Lett. 82 (1999) 271-276, hep-ex/9810029

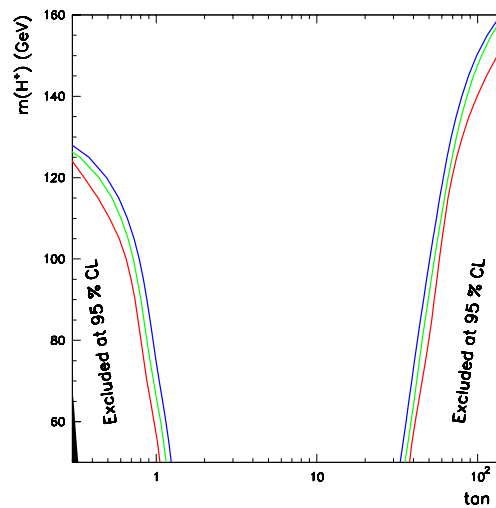


**Figure 11:** The 95% C.L. exclusion contours for charged higgs production ( $m_t = 175$   $\text{GeV}/c^2$ ). The hatched area with solid outlines is  $\sigma(t\bar{l}) = 5.3$  pb, the dashed lines are 5.0 pb, and the dotted lines are 4.5 pb.

- [8] Phys.Rev. D58 (1998) 052001, hep-ex/9802018 and Phys.Rev. D60 (1999) 052001, hep-ex/9808029
- [9] Catani et al., Phys.Lett. B378 (1996) 329-336, hep-ph/9602208
- [10] The Combined Mass Paper
- [11] H. Singh, Ph.D. thesis, University of California Riverside, Riverside, 1999.

- 
- [12] The DZERO Collaboration, Neural Networks for Analysis of Top Quark Production, Lepton-Photon 99 Proceedings, FERMI-CONF-99-206-E, hep-ex/9907041.
  - [13] J.F. Gunion, H.E. Haber, G. Kane, and S. Dawson, *The Higgs Hunter's Guide* Addison-Wesley, New York, 1990.
  - [14] D0 Collaboration (B. Abbot et al.), *Phys. Rev. Lett.* 82, 4975 (1999).
  - [15] D0 Collaboration (S. Abachi et al.), *Phys. Rev. Lett.* 79, 1203 (1997).
  - [16] C. Hill and S. Parke, *Phys. Rev. D* 49, 4454-4462 (1994)
  - [17] Rizzo, *Phys. Rev. D* 59 115010 (1999)
  - [18] S. Choi, Ph.D. thesis, Seoul National University, Seoul, Korea, 1999.
  - [19] T. Stelzer and S. Willenbrock, *Phys. Lett. B* 374, 169 (1996); K.Y. Lee, H.S. Song, J. Song, and C. Yu, Report No. SNUTP-99-022 (1999), hep-ph/9905227; G. Mahlon and S. Parke, *Phys. Rev. D* 53, 4886 (1996).
  - [20] G. Mahlon and S. Parke, *Phys. Lett. B* 411, 173 (1997).
  - [21] dzero Collaboration (B. Abbot et al.), *Phys. Rev. Lett.* 82, 4975 (1997)
  - [22] The CLEO Collaboration *Phys. Rev. Lett.* 49 357 (1982).
  - [23] M. Takita, Recent results from the Super-Kamiokande, ICHEP98 Proceedings
  - [24] Summary of the Electroweak working group at CERN, CERN-EP/99-15
  - [25] T. Stelzer, Z. Sullivan, and S. Willenbrock, Single-top-quark production at hadron colliders, *Phys. Rev. D* 58 (1998) 094021, hep-ph/9807340
  - [26] A. Barbaro-Galtieri, Proceedings of the 1999 Lathuile Conference. FERMI-LAB-CONF-99/246-E, hep-ph/0009016
  - [27] Arkani-Hamed et al., The Hierarchy Problem and New Dimensions at a Millimeter, *Phys. Lett. B* 429 (1998) 263-272, hep-ph/9803315.
  - [28] CDF pt measurements